



**HAL**  
open science

## Near-infrared emission in Er- and Pr-doped YSZ crystalline superlattices

Alicia Ruiz-Caridad, Joan Manel Ramírez, Elena Duran-Valdeiglesias,  
Guillaume Marcaud, Xavier Le Roux, Carlos Alonso Ramos, Thomas  
Maroutian, Sylvia Matzen, Eric Cassan, Delphine Marris-Morini, et al.

► **To cite this version:**

Alicia Ruiz-Caridad, Joan Manel Ramírez, Elena Duran-Valdeiglesias, Guillaume Marcaud, Xavier Le Roux, et al. Near-infrared emission in Er- and Pr-doped YSZ crystalline superlattices. *Journal of Luminescence*, 2022, 246, pp.118844. 10.1016/j.jlumin.2022.118844 . hal-03869608

**HAL Id: hal-03869608**

**<https://hal.science/hal-03869608>**

Submitted on 24 Nov 2022

**HAL** is a multi-disciplinary open access archive for the deposit and dissemination of scientific research documents, whether they are published or not. The documents may come from teaching and research institutions in France or abroad, or from public or private research centers.

L'archive ouverte pluridisciplinaire **HAL**, est destinée au dépôt et à la diffusion de documents scientifiques de niveau recherche, publiés ou non, émanant des établissements d'enseignement et de recherche français ou étrangers, des laboratoires publics ou privés.

# Near-infrared emission in Er- and Pr-doped YSZ crystalline superlattices

Alicia Ruiz-Caridad<sup>1,\*</sup>, Joan Manel Ramírez<sup>2</sup>, Elena Duran-Valdeiglesias<sup>3</sup>, Guillaume Marcaud<sup>4</sup>, Xavier Le Roux<sup>1</sup>, Carlos Alonso Ramos<sup>1</sup>, Thomas Maroutian<sup>1</sup>, Sylvia Matzen<sup>1</sup>, Eric Cassan<sup>1</sup>, Delphine Marris-Morini<sup>1</sup>, Philippe Lecoœur<sup>1</sup>, Laurent Vivien<sup>1</sup>.

<sup>1</sup> Université Paris-Saclay, CNRS, Centre de Nanosciences et Nanotechnologies (C2N), UMR 9001, 10 Boulevard 29 Thomas Gobert, 91120 Palaiseau, France.

<sup>2</sup> III-V lab, 1 Avenue Augustin Fresnel, 91767 Palaiseau Cedex, France

<sup>3</sup> Almae Technologies, Route de Nozay, 91460 Marcoussis, France

<sup>4</sup> Yale University, Department of applied physics, 15 prospect street, 06511 New Haven, CT, USA

\*Corresponding author: e-mail address: alicia.ruiz-caridad@u-psud.fr

Revised accepted version, February 2022

## Abstract

Broadband on-chip light amplifier is one of the key building blocks for the development of integrated circuits for datacom and telecom applications. In this context, the article reports on the near-IR emission properties of rare-earth doped crystalline thin layers of Y<sub>2</sub>O<sub>3</sub>-ZrO<sub>2</sub> (YSZ): Er-doped YSZ, Pr-doped YSZ and a superlattice of Er- and Pr- doped YSZ. Absorption studies proved differences in wavelengths in superlattice sample with Pr<sup>3+</sup> and Er<sup>3+</sup> in comparison with Er-doped YSZ and Pr-doped YSZ monolayers. Power efficiency was determined for all samples, revealing larger emission and higher optical efficiency for Er<sup>3+</sup> ions at 1530 nm (C-band) than Pr<sup>3+</sup> emission at 1350 nm (O-band) in the superlattice sample. Simultaneous emission from Er<sup>3+</sup> and Pr<sup>3+</sup> ions was observed by exciting the Er- and Pr-doped YSZ superlattice in a range from 980 to 1000 nm wavelengths. Besides, energy transfer from Pr<sup>3+</sup> to Er<sup>3+</sup> was demonstrated in the superlattice sample containing Pr<sup>3+</sup> and Er<sup>3+</sup> ions.

## Keywords

Erbium, Praseodymium, superlattice, near-IR emission, photoluminescence

## Introduction

Silicon photonics has generated a great interest addressing challenges for datacom and telecom applications in the O-band and C-band, respectively [1,2,3]. Silicon photonics faces some limitations in silicon photonics such indirect bandgap and light absorption in the mid-IR. One of the main aims in silicon circuits is on-chip optical amplification. Due to its indirect bandgap, light emission from silicon (Si) is very weak [4]. As a result, efforts are currently put into developing

and engineering new materials and structures for hybrid integration onto silicon photonic platforms. Thus, additional materials suitable for light emission, sensing or adding functionalities are required to hybridize in the silicon photonics platform.

Among materials compatible with CMOS technology, rare-earth doped oxides are well-known luminescent materials, widely used in optoelectronics, as optical amplifiers and for sensing applications [5, 6, 7, 8].

In this work, we aim to explore the emission behavior in the near infrared (near-IR) wavelengths range at both the O-band (1260-1360 nm) and the C-band (1530-1565 nm) of the optical communications windows for integrated optical amplification in silicon photonics platform.

As rare-earth (RE) materials, praseodymium ( $\text{Pr}^{3+}$ ) and erbium ( $\text{Er}^{3+}$ ) ions are good candidates for emissions around 1300 and 1550 nm, respectively [9]. First,  $\text{Pr}^{3+}$  has been successfully used as optical amplifier at 1300 nm ( $\text{Pr}^{3+}$  transition at  $^1\text{G}_4 \rightarrow ^3\text{H}_5$ ) in Pr-doped fibers [10,11] and as doping in hosts such as glasses in waveguides for amplification and lasing in the near-IR and visible range of wavelengths [12,13]. Second,  $\text{Er}^{3+}$  transition  $^4\text{I}_{13/2} \rightarrow ^4\text{I}_{15/2}$  has been largely studied for optical amplification and lasing purposes in a wide range of amorphous and crystalline host materials [14]. Latest results on optical amplification proved large net modal gain of  $\sim 20$  dB/cm and signal enhancement of  $\sim 19$  dB for  $\text{Er}^{3+}$ -doped  $\text{Al}_2\text{O}_3$  [15,16]. Besides,  $\text{Pr}^{3+}$  and  $\text{Er}^{3+}$  codoping studies in proved ion emission at both O- and C- band region of wavelengths with applications in the fields of optical communications, optical amplification in fibers, and sensing [17, 18, 19]. Recently,  $\text{Pr}^{3+}$  and  $\text{Er}^{3+}$  codoping glasses demonstrated broadband emission in the near-IR wavelengths at ultraviolet (UV) pumping wavelengths [20, 21].

One of the main challenges in hybrid integration platforms of crystalline materials is lattice mismatch hindering epitaxial growth on silicon and introducing defects. Materials engineering for hybrid integration on silicon platforms are the key to address this limitation and adding other functionalities. For this purpose, functional oxides summon attention by its outstanding properties including superconductivity, magnetism, ferroelectricity, catalytic activity, resistive switching, electro-optic effects, piezoelectricity, or optical nonlinearities [22]. In this context, we report on the light emission characteristics of rare-earth (RE) doped crystalline oxide layers. As oxide layer, yttria-stabilized zirconia (YSZ) can be epitaxially integrated on Si, hence making YSZ an efficient buffer layer upon which several functional crystalline oxides can be grown [23]. Moreover, YSZ is a promising host matrix for rare-earth materials in photonics as it is transparent from the ultraviolet (UV) to the middle infrared (mid-IR), has a good mechanic and chemical stability and has a large bandgap that prevents two-photon absorption (TPA) [24, 25].

Moreover, previous works reveal YSZ as an outstanding photonic material with low propagation losses (3 dB/cm) on waveguides [26], nonlinear properties and signal enhancement in the C-band wavelengths for Er-doped YSZ [27].

In this work, we achieve simultaneous  $\text{Pr}^{3+}$  and  $\text{Er}^{3+}$  emission at wavelengths of 1350 nm and 1530 nm under excitation of a crystalline Er- and Pr-doped YSZ (Er:Pr:YSZ) superlattice thin-film. Superlattice structure is expected to minimize  $\text{Pr}^{3+}/\text{Er}^{3+}$  ion-ion interaction. Furthermore, we will discuss emission intensity and optical efficiency of  $\text{Pr}^{3+}$  and  $\text{Er}^{3+}$  ion emission from the superlattice

compared with Pr-doped YSZ (Pr:YSZ) or Er-doped YSZ (Er:YSZ) monolayers. Finally, we will reveal energy transfer from Pr<sup>3+</sup> to Er<sup>3+</sup> ions.

## 2. Experimental details

Thin film crystalline RE-doped YSZ samples are grown by pulsed laser deposition (PLD) on C-cut sapphire (Al<sub>2</sub>O<sub>3</sub>) substrate. In this regard, we employed four commercial sintered targets fabricated by TOSHIMA Manufacturing Co. with Er<sup>3+</sup> concentrations of: 0.5, 1.5 and 3 at. % in Er:YSZ and 0.5 at. % of Pr<sup>3+</sup> in Pr:YSZ. YSZ is grown in cubic phase using 8 mol % of Y<sub>2</sub>O<sub>3</sub> providing structural stability. Furthermore, YSZ cubic crystalline structure and lattice constant ( $a_{\text{YSZ}} = 5.15 \text{ \AA}$ ) similar to silicon's Si ( $a_{\text{Si}} = 5.43 \text{ \AA}$ ) allow for future epitaxial implementation of YSZ on Si for hybrid integration [28]. Thus, 150 nm-thick monolayers and a 300 nm-thick superlattice are deposited for all Er<sup>3+</sup> and Pr<sup>3+</sup> target compositions. A 5 Hz repetition rate, KrF excimer laser at a wavelength of 248 nm and at an incident optical fluence of 3 J/cm<sup>2</sup> is used for the ablation of the rotating sintered RE-doped YSZ target under an incident angle of 45°. Sapphire (Al<sub>2</sub>O<sub>3</sub>) substrate is placed on a heated holder at 50 mm from the targets and heated from room temperature to 800 °C at a rate of 10 °C/min at an initial pressure of 10<sup>-6</sup> Torr. The chamber receives a constant flux of oxygen at a pressure of 30 mTorr during deposition. After deposition, the substrate is cooled down at a rate of 10 °C/min under oxygen atmosphere at 300 Torr pressure.

Structural characterization by X-ray diffraction (XRD) was performed in an X-ray diffractometer model X'Pert Pro from PANalytical in parallel beam configuration with monochromated Cu K<sub>α</sub>1 radiation (wavelength of 1.540598 Å) to determine crystalline quality of thin film samples.

Thereafter, we performed optical characterization by photoluminescence (PL). Among other emission measurements, PL technique allows to determine the most efficient wavelength to excite rare-earth ions in a host. In this study, we pumped thin films using a continuous wave (CW) tunable Ti:sapphire laser (wavelengths from 600 to 1050 nm) in perpendicular incidence to the surface of the sample using a microscope objective with a 50X magnification and a NA of 0.55 which generates an excitation beam radius of ~ 1.5 μm. Emission signals are perpendicularly collected by the same microscope objective and focused to the detector. Pump wavelength is filtered with a high-pass filter (1100 nm) and only emission in near-IR is detected by a nitrogen-cooled-detector through a iHR320 spectrometer.

## 3. Results and discussion

### 3.1. X-ray diffraction (XRD)

X-ray diffraction (XRD) was performed to study the crystallinity in three thin film samples grown on a sapphire substrate: (i) 0.5 at. % Pr:YSZ monolayer, (ii) 0.5 at. % Er:YSZ monolayer and (iii) superlattice with Er: and Pr:YSZ in its structure. The analysis by XRD shows two diffraction peaks at 30° and 35° corresponding to two YSZ cubic crystalline orientations: (111) and (001) [29].

Besides, in the  $2\theta$  diffraction scans we observed a sharp diffraction intensity at  $42^\circ$  from the (0006) family of planes of C-cut sapphire substrate. In Fig. 1 (a), XRD measurement for Pr:YSZ thin film presents two crystalline orientations: (111) and (001). Similarly, for both 0.5 at. % Er:YSZ monolayer and Er:Pr:YSZ superlattice samples intensity diffraction peaks (Fig. 1(b) and (c)) are found at (001) and (111) orientations from YSZ cubic structure, as expected. XRD intensities quantify the presence of domains of YSZ grown in a (001) or (111) orientation of the cubic structure of YSZ. The relative contributions from (001) and (111) crystalline orientations are observed to change between the three types of sample, probably due to slightly different composition-dependent behaviors during growth. For all three samples, the XRD analysis reveals high crystalline quality thin film of RE-substituted YSZ in cubic phase.

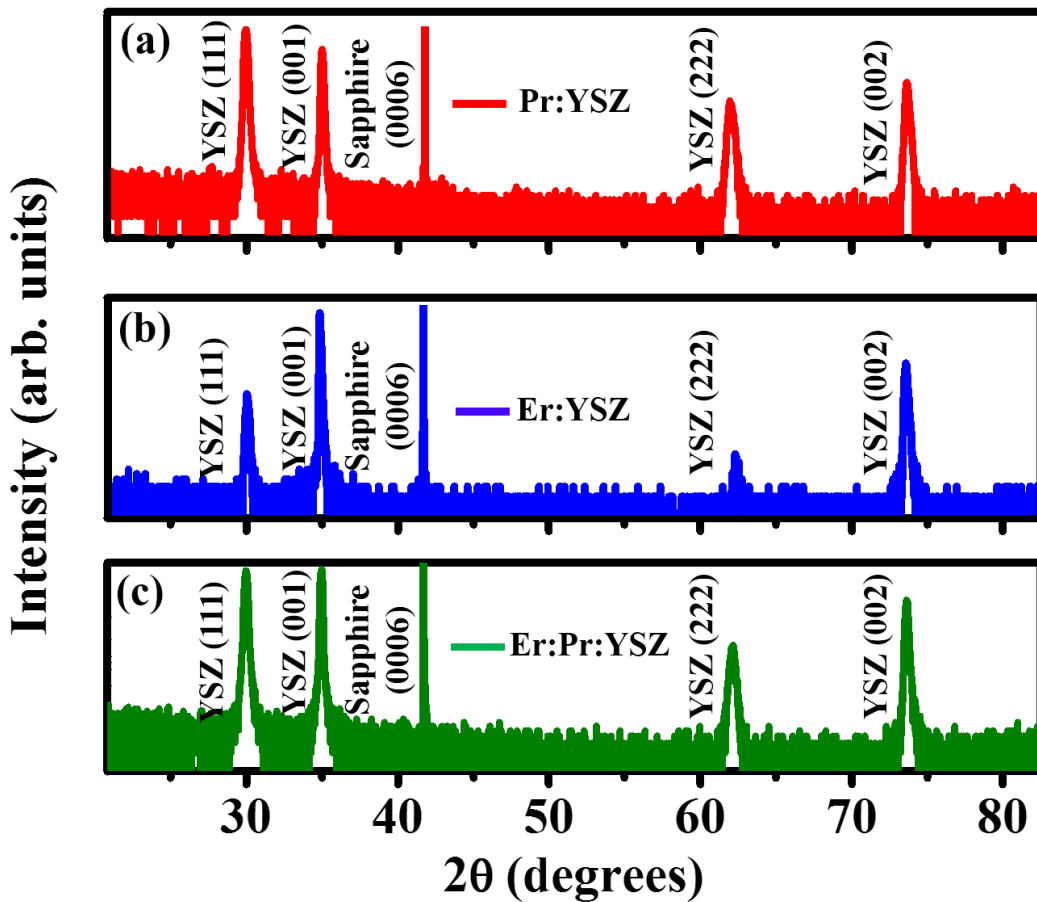


**Figure 1.** X-ray diffraction  $\theta$ - $2\theta$  scans from top to bottom: (a) Pr:YSZ, (b) Er:YSZ monolayers and (c) Er:Pr:YSZ superlattice.

### 3.2. Optical properties

In our work, we aim to develop an optical efficient photonic material whose emission range lies in both the O-band (1250-1350 nm) and the C-band (1530-1565 nm) to be implemented as light amplifier for datacom and telecom applications. With this purpose, we were interested to study two RE transitions  $^1G_4 \rightarrow ^3H_5$  and  $^4I_{13/2} \rightarrow ^4I_{15/2}$  corresponding to emission wavelengths of 1350 nm

and 1530 nm of  $\text{Pr}^{3+}$  and  $\text{Er}^{3+}$  ions, respectively [30,31]. By growing a Er:Pr:YSZ superlattice we aim to implement  $\text{Pr}^{3+}$  and  $\text{Er}^{3+}$  ions in the same sample. Besides, the construction of a superlattice allows a higher control of  $\text{Er}^{3+}$  and  $\text{Pr}^{3+}$  interdistances, diminishing ion-ion interaction.

In this regard, to determine optimal RE concentration to avoid quenching effects which hinders luminescence, we performed a PL study on Er:YSZ monolayers at 0.5, 1.5 and 3 at. % of  $\text{Er}^{3+}$ .

PL optical efficiency studies of three 150 nm-thick Er:YSZ films with  $\text{Er}^{3+}$  ion concentrations at 0.5, 1.5 and 3 at. % were measured in Fig. 2. Optical efficiency ( $\epsilon$ ) is defined as the ratio between intensity emission and pumping power. In order to estimate  $\text{Er}^{3+}$  concentration with lower quenching effects, we measured the PL intensity of  $\text{Er}^{3+}$  emission at 1530 nm with pumping power (0-120 mW) at 960 nm wavelength, and we calculated the curve slope or optical efficiency. In Fig. 2, we can notice higher slope (and thus a higher optical efficiency) for the Er:YSZ sample doped with  $\text{Er}^{3+}$  ion concentration at 0.5 at. %. Higher optical efficiency is directly related to lower quenching effects. Higher ion concentration increases ion-ion interaction, which is actually one of the main quenching mechanisms in RE samples. Consequently, we observe in Fig. 2 that curve slope corresponding to sample containing  $\text{Er}^{3+}$  ions at 1.5 at. % is lower than curve slope for sample at  $\text{Er}^{3+}$  at 0.5 at. %, revealing lower efficiency and hindering of luminescence for 1.5 at. %  $\text{Er}^{3+}$  sample. Quenching effect is further evidenced in samples containing  $\text{Er}^{3+}$  at 3 at. % in which the slope observed in Fig. 2 is the lowest. In addition, PL emission saturation is observed for pumping power values from 105 mW. In summary, we have measured the highest optical efficiency ( $\epsilon_{\text{Er:YSZ}}=0.9$ ), thus low quenching effects for 0.5 at. % Er:YSZ monolayers, proving this concentration to be optimal in YSZ hosts for photonic purposes.

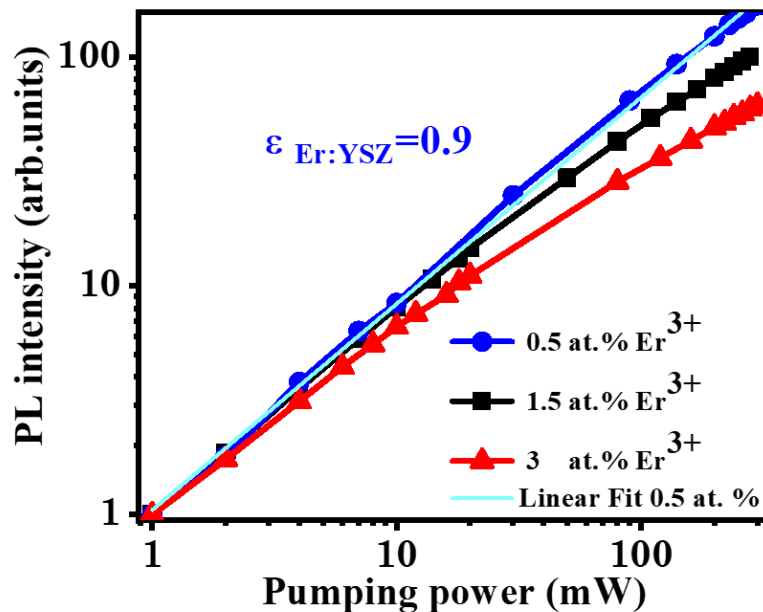


**Figure 2.** PL intensity as a function of the pump power of Er:YSZ monolayer thin films with Er<sup>3+</sup> at. % of 0.5, 1.5 and 3 at. % in blue, black and red, pumping at 960 nm and Er<sup>3+</sup> emission at 1530 nm wavelength. Highest optical efficiency ( $\epsilon_{\text{Er:YSZ}} = 0.9$ ) and linear fit is achieved for 0.5 at. % Er:YSZ monolayer.

After Er<sup>3+</sup> ion emission PL results, we explored optical efficiency of 0.5 at. % Pr:YSZ. Er-:Pr-co-doping studies in the literature for optical applications in the near-IR have determined 0.5 at. % Pr:YSZ as most efficient concentration for 0.5 at. % Er<sup>3+</sup> co-doping [32]. For this reason, we will use Pr<sup>3+</sup> and Er<sup>3+</sup> concentrations of 0.5 at. % to grow our superlattice sample. In Fig. 3 we show optical efficiency of the 0.5 at. % Pr:YSZ monolayer. In this study, we observed optical efficiency for 0.5 at. % Pr:YSZ at 1350 nm emission ( $\epsilon_{\text{Pr:YSZ}} = 0.53$ ) remains lower than previous calculations for 0.5 at.% Er:YSZ monolayer thin films measured at 1530 nm ( $\epsilon_{\text{Er:YSZ}} = 0.9$ ). Further studies of optical efficiency will be presented in the last part of the manuscript.

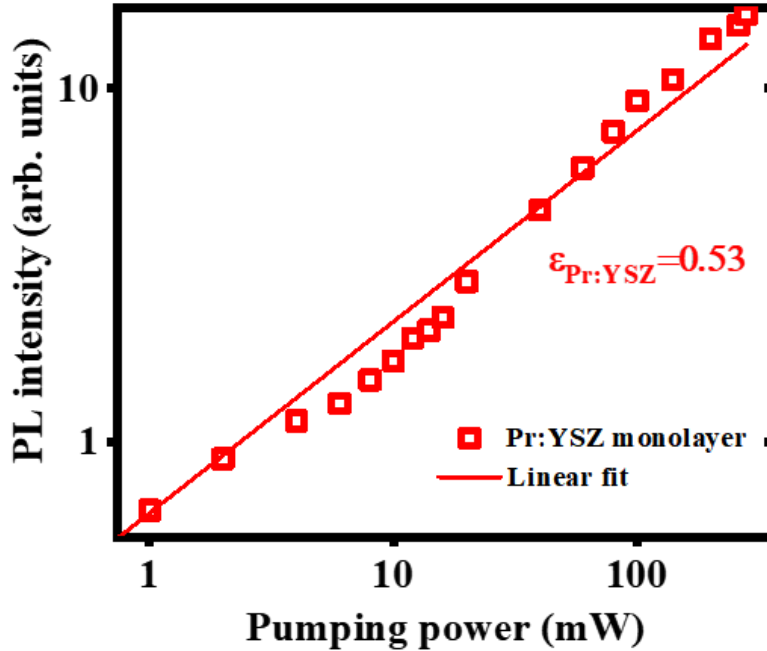


**Figure 3.** Optical efficiency ( $\epsilon_{\text{Pr:YSZ}} = 0.53$ ) for 0.5 at. % Pr:YSZ monolayer pumped at 1020 nm and Pr<sup>3+</sup> emission at 1350 nm wavelength.

From these preliminary results on Er:YSZ and Pr:YSZ monolayers, we have grown a superlattice sample made by alternating of 3 nm-thick layer of 0.5 at. % Er:YSZ and 0.5 at. % Pr:YSZ layers to explore Pr<sup>3+</sup> and Er<sup>3+</sup> emission at 1350 and 1530 nm, respectively (Fig. 4). Superlattices were made to homogeneously distribute Er<sup>3+</sup> and Pr<sup>3+</sup> ions in the host while vertically controlling ion interdistances, limiting quenching effects.

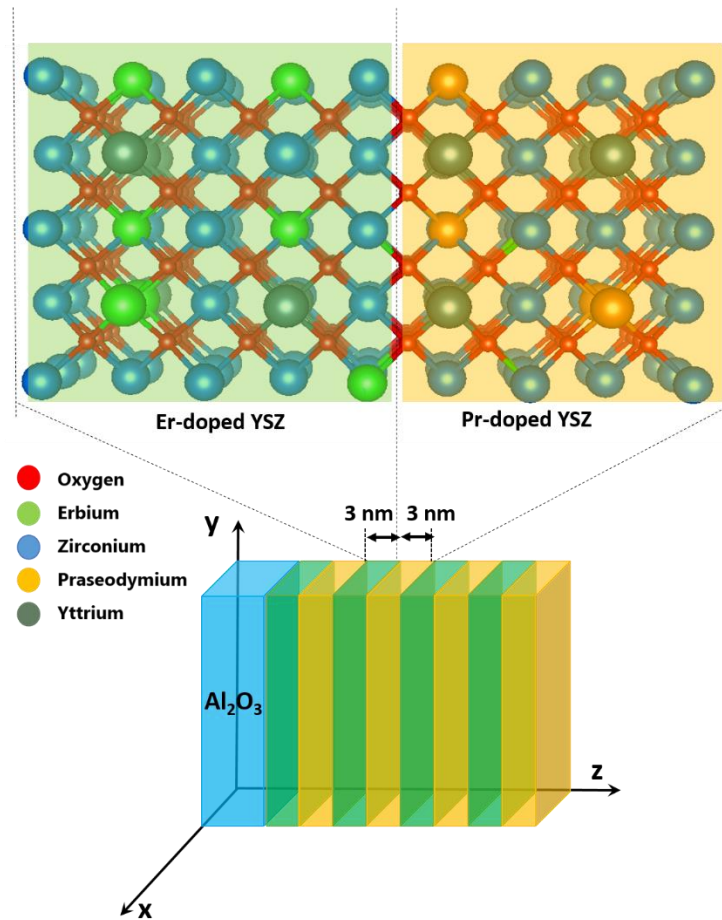


**Figure 4.** Schematic crystalline configuration of a superlattice of Er- (3 nm thickness) and Pr- (3 nm thickness) doped YSZ in green and orange, respectively, on an  $\text{Al}_2\text{O}_3$  substrate in blue.

### 3.2.1. Absorption pumping wavelength

To determine the optimal  $\text{Pr}^{3+}$  and  $\text{Er}^{3+}$  absorption wavelengths of three thin film samples (0.5 at. % Pr:YSZ, 0.5 at.%, Er:YSZ, and a superlattice with 0.5 at. % Er:Pr:YSZ), we excited our samples with a tunable Ti:sapphire laser a range of wavelengths between 760-1050 nm at a fix pumping power of 40 mW. Results from this study prove highest absorption wavelength of Pr:YSZ sample at 1030 nm corresponding to the  $\text{Pr}^{3+}: {}^5\text{H}_4 \rightarrow {}^1\text{G}_4$  transition (Fig. 5 (a)). While the optimal absorption for Er:YSZ samples is obtained for the  $\text{Er}^{3+}: {}^4\text{I}_{15/2} \rightarrow {}^4\text{I}_{11/2}$  transition at a wavelength of 960 nm (Fig. 5 (b)). Unexpectedly, for Er:Pr:doped YSZ superlattice thin film, highest absorption wavelengths from  $\text{Er}^{3+}$  and  $\text{Pr}^{3+}$  ions are obtained by pumping the sample at wavelengths of 970 and 1020 nm, respectively (Fig. 5 (c) and (d)). It can be noticed a shift of  $\pm 10$  nm in both pumping wavelengths from  $\text{Er}^{3+}$  and  $\text{Pr}^{3+}$  in superlattice configuration in comparison with optimal absorption wavelengths of Er:YSZ and Pr:YSZ monolayers. Indeed, maximum  $\text{Er}^{3+}$  PL emission at 1530 nm from superlattice sample is observed at a pumping wavelength of 970 nm, which is  $\sim 10$  nm above the optimal pumping wavelength for Er:YSZ monolayer ( $\lambda_{\text{Er:YSZ}} = 960\text{nm}$ ). On the contrary, maximum  $\text{Pr}^{3+}$  PL intensity emission at 1350 nm from the same superlattice sample is

observed when pumping the superlattice at 1020 nm wavelength,  $\sim 10$  nm below the optimal wavelength for Pr:YSZ monolayer ( $\lambda_{\text{Pr:YSZ}} = 1030$  nm). Despite the minute shift of  $\sim 10$  nm, we will perform optical characterization of each sample at its optimal absorption wavelength to equally compare optical efficiency and PL intensity among samples. RE absorption and emission wavelengths are host's crystal-fields energy dependent [33]. Absorption and emission spectra are determined by the site RE takes in matrix structure [34]. Thus, differences in absorption wavelengths of  $\text{Er}^{3+}$  and  $\text{Pr}^{3+}$  between monolayer samples and superlattice structure can probably be explained by changes in the crystal-field structure of the host due to the presence of two different dopants.

Finally, we observed in Fig. 5 (c) and (d) for Er:Pr:YSZ sample absorption overlap for  $\text{Er}^{3+}$  and  $\text{Pr}^{3+}$  PL profiles from wavelengths of 970 to 1020 nm. Thus, we are able to simultaneously generate photon emission from  $\text{Er}^{3+}$  and  $\text{Pr}^{3+}$  at 1530 and 1350 nm by pumping within this wavelength range.

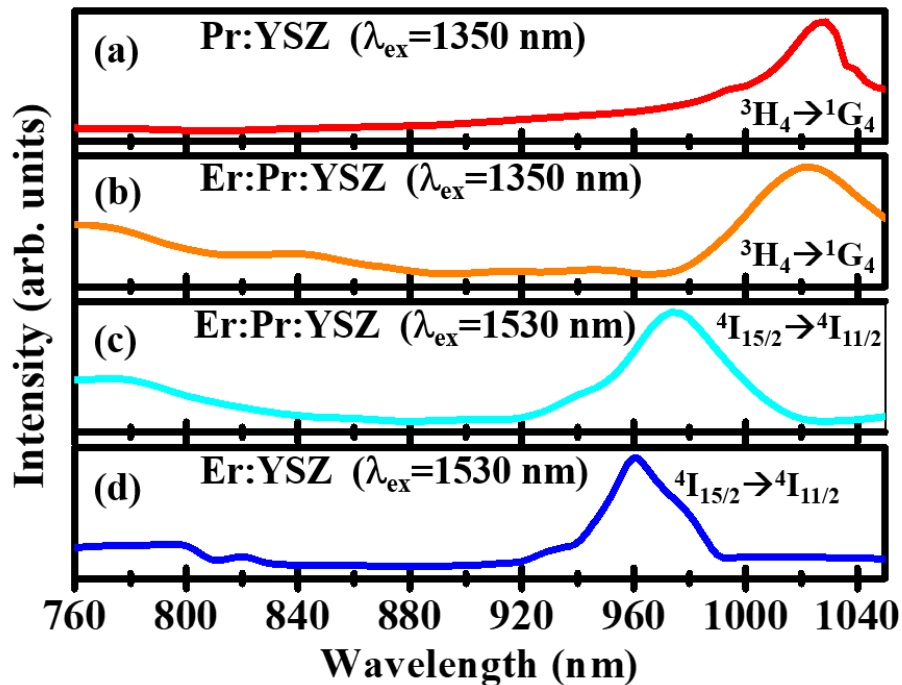


**Figure 5.** PL absorption intensity of (a) Pr:YSZ, (b)  $\text{Pr}^{3+}$  in Er:Pr:YSZ,  $\text{Er}^{3+}$  in (c) Er:Pr:YSZ and (d) Er:YSZ thin films.

### 3.2.2. PL emission properties

After absorption studies for the three samples, we performed PL measurements to explore ion emission profile at pump power fixed to 20 mW to ensure that we avoid nonlinear phenomena. We started by exciting the superlattice sample at wavelengths of 970 and 1020 nm proving  $\text{Er}^{3+}$  and  $\text{Pr}^{3+}$  emission spectra at wavelengths of 1530 and 1350 nm, respectively (Fig. 6).

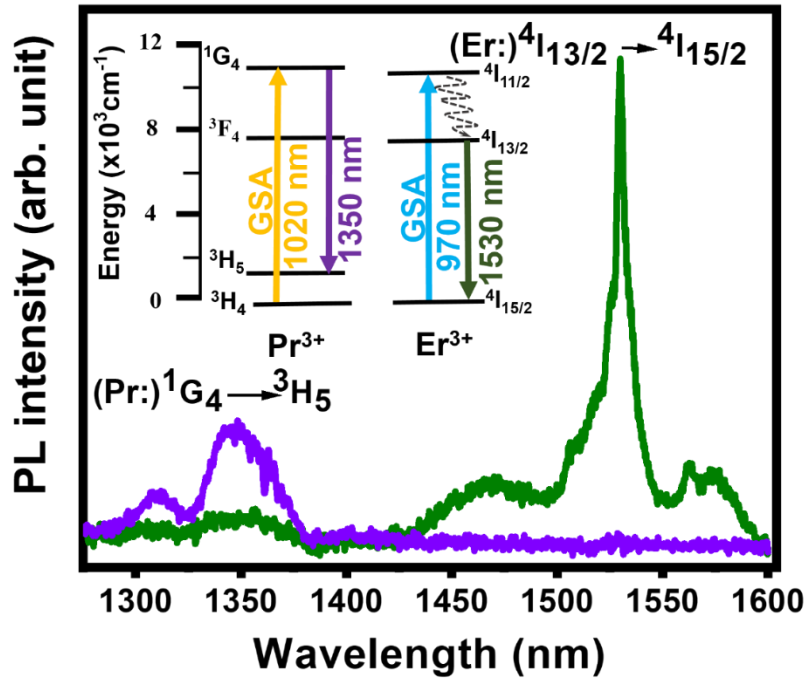


**Figure 6.** PL emission profile of  $\text{Pr}^{3+}$  (violet) and  $\text{Er}^{3+}$  (green) ions in Er:Pr:YSZ. Inset, schematics of energy levels for ground state absorption (GSA) and emission in the near-IR of  $\text{Pr}^{3+}$  (orange and violet) and  $\text{Er}^{3+}$  (blue and green) ions.

The evolution of PL emission from ( $\text{Er}^{3+}$ ):  ${}^4\text{I}_{13/2} \rightarrow {}^4\text{I}_{15/2}$  and ( $\text{Pr}^{3+}$ ):  ${}^1\text{G}_4 \rightarrow {}^3\text{H}_5$  transitions in the Er:Pr:YSZ superlattice sample has been performed by pumping the sample from 750 to 1050 nm (Fig. 7(a)). We detected stronger emission at wavelengths of 970 nm and 1020 nm from  $\text{Er}^{3+}$  and  $\text{Pr}^{3+}$  ions, respectively. As expected, under pump wavelengths of 970 nm and 1020 nm, we only obtain a PL profile corresponding to  $\text{Er}^{3+}$  transition ( ${}^4\text{I}_{13/2} \rightarrow {}^4\text{I}_{15/2}$ ) at a wavelength of 1530 nm and  $\text{Pr}^{3+}$  transitions ( ${}^1\text{G}_4 \rightarrow {}^3\text{H}_5$ ) at a wavelength of 1350 nm, respectively (Fig. 7(b)). In order to prove simultaneous emission at 1530 and 1350 nm from both  $\text{Er}^{3+}$  and  $\text{Pr}^{3+}$  ions, we excited Er:Pr:YSZ superlattice sample at two wavelengths between 970 and 1020 nm: 980 and 1000 nm as shown in Fig. 7(b). Under an excitation wavelength of 980 nm, simultaneous emissions from  ${}^4\text{I}_{13/2} \rightarrow {}^4\text{I}_{15/2}$  ( $\text{Er}^{3+}$ ) and  ${}^1\text{G}_4 \rightarrow {}^3\text{H}_5$  ( $\text{Pr}^{3+}$ ) at 1350 and 1530 nm are effectively observed with highest emission intensity for  $\text{Er}^{3+}$  emission due to higher absorption of  $\text{Er}^{3+}$  at this wavelength. At a pump wavelength of 1000 nm, similar PL intensities are obtained at both 1350 nm and 1530 nm emissions. Thus, simultaneous  $\text{Pr}^{3+}$  and  $\text{Er}^{3+}$  emission at 1350 and 1530 nm has been proved in the superlattice sample for pumping wavelengths between 980 and 1000 nm.

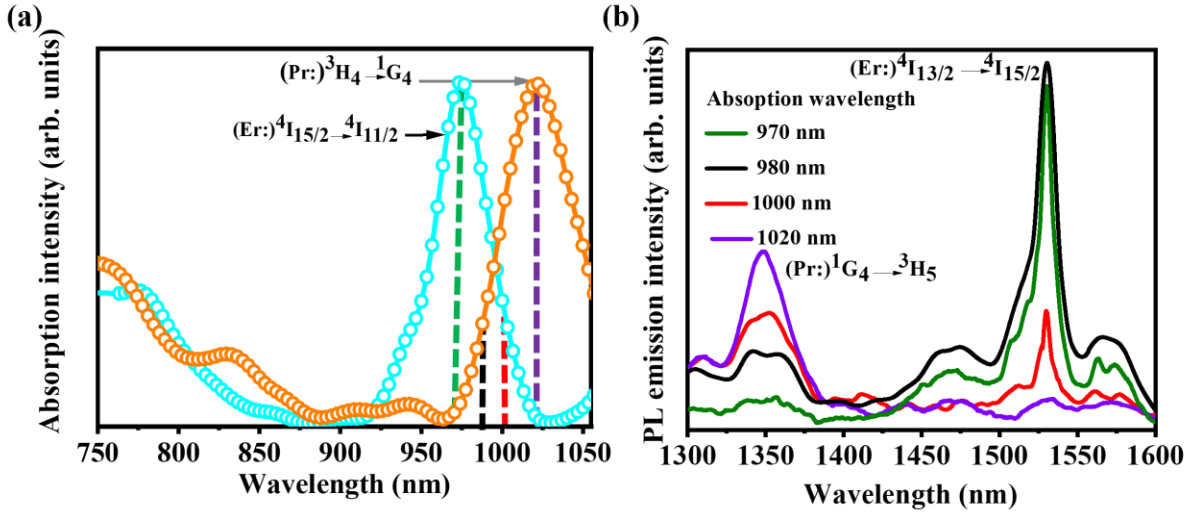


**Figure 7.** Er:Pr:YSZ superlattice PL profiles: (a) absorption profile for Er<sup>3+</sup> and Pr<sup>3+</sup> transitions, (b) PL emission spectra corresponding to 4 excitation wavelengths: 970, 980, 1000 and 1020 nm.

Finally, we pumped by PL Er:YSZ and Pr:YSZ monolayers at 970 and 1030 nm to compare Er<sup>3+</sup> and Pr<sup>3+</sup> PL spectra from superlattice sample with Pr:YSZ (Fig. 8 (a)) and Er:YSZ monolayers' (Fig. 8 (b)) PL emission. Fig. 8 (a) reports Er:Pr:YSZ superlattice and Pr:YSZ monolayer samples' PL profile pumped at wavelengths of 1020 and 1030 nm, respectively. Despite similarities in PL emission intensity profiles corresponding to the <sup>1</sup>G<sub>4</sub> → <sup>3</sup>H<sub>5</sub> transition at 1350 nm for both samples, PL intensity for Pr:YSZ sample has been proved higher than superlattice emission. On the Er<sup>3+</sup> emission spectra (Fig. 8 (b)) from both Er:YSZ and superlattice samples under pumping wavelength of 960 and 970 nm, respectively, only one intensity peak from Er<sup>3+</sup> PL profile at 1530 nm from <sup>4</sup>I<sub>13/2</sub> → <sup>4</sup>I<sub>15/2</sub> transition has been measured in the wavelength range from 1300 to 1600 nm. We also observe, as for samples with Pr<sup>3+</sup> ions, similar PL signal profile for both Er<sup>3+</sup> samples with higher intensity for Er:YSZ sample.

Despite the mild shift observed in the absorption study for Er<sup>3+</sup> and Pr<sup>3+</sup> in the superlattice in comparison with Er:YSZ and Pr:YSZ monolayers, PL emission spectra of both RE in monolayers and superlattice in the near-IR wavelengths remain very similar. However, we observed an increase of PL intensity for Pr:YSZ and Er:YSZ with respect Er:Pr:YSZ emission. These results suggest luminescence is hindered in Er:Pr:YSZ superlattice emission due to ion-ion interaction between Er<sup>3+</sup> and Pr<sup>3+</sup> ions.

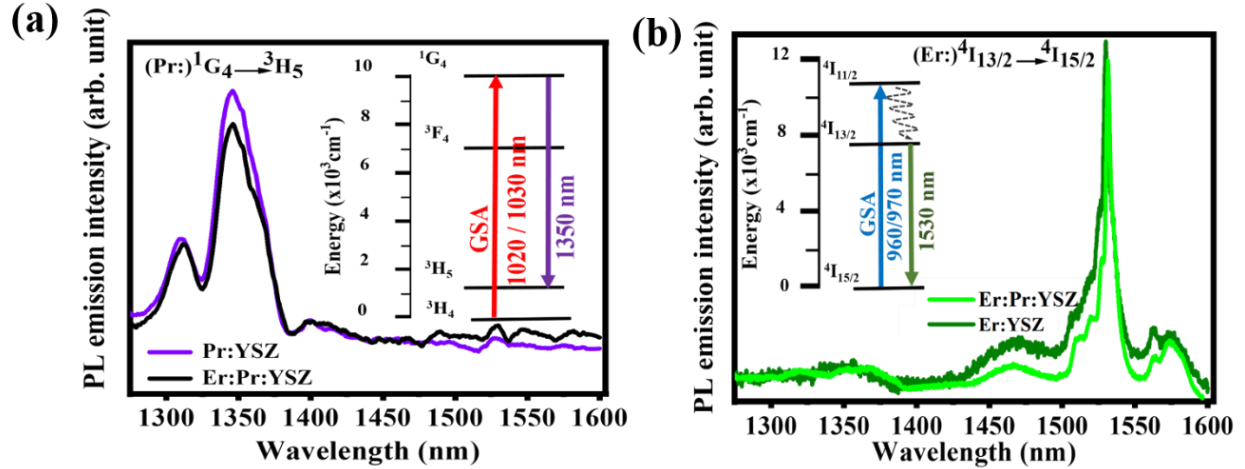


**Figure 8.** a) PL emission profile of  $\text{Pr}^{3+}$  ions in Pr:YSZ (violet) and Er:Pr:YSZ (black). Inset, schematics of energy levels for absorption transition for ground state absorption (GSA) and emission in the near-IR. b) PL emission profile of  $\text{Er}^{3+}$  ions in Er:YSZ (dark green) and in Er:Pr:YSZ (light green). Inset, schematics of energy levels for absorption and emission in the near-IR of  $\text{Er}^{3+}$  ions.

For clarity, we include in Table 1 absorption and emission transitions and wavelengths of  $\text{Er}^{3+}$  and  $\text{Pr}^{3+}$  measured for the three samples.

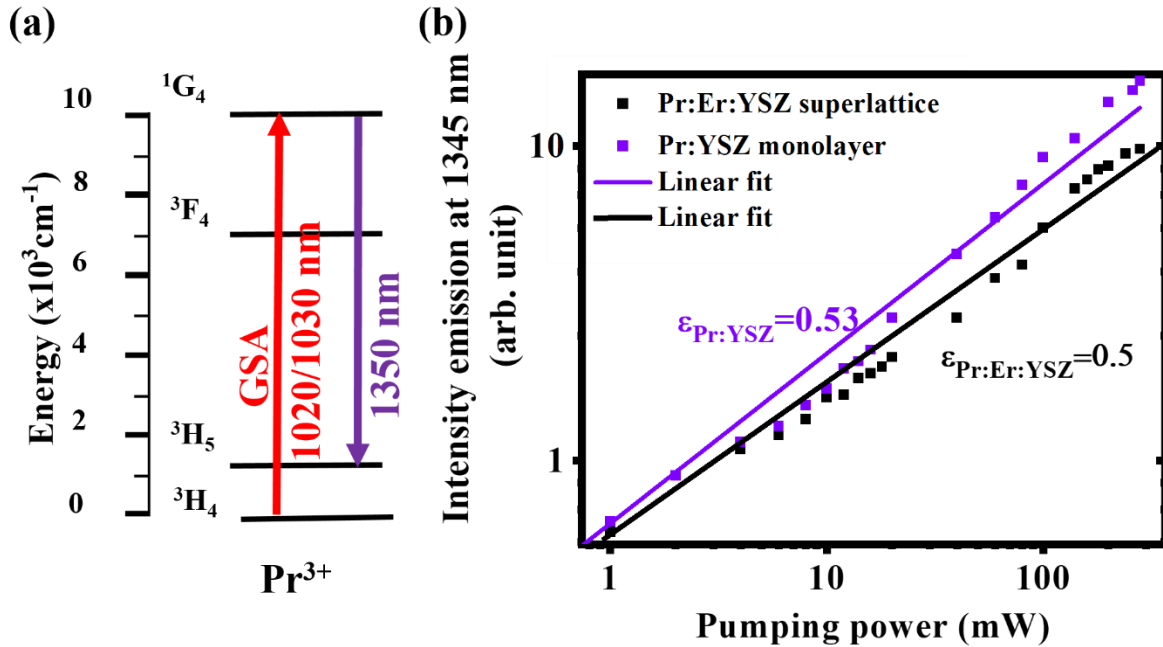
Sample name	Composition	Absorption transition	Absorption wavelength (nm)	Emission transition	Emission wavelength (nm)
#1	Er:YSZ	$^4\text{I}_{15/2} \rightarrow ^4\text{I}_{11/2}$	960	$^4\text{I}_{13/2} \rightarrow ^4\text{I}_{15/2}$	1530
#2	Pr:YSZ	$^3\text{H}_4 \rightarrow ^1\text{G}_4$	1030	$^1\text{G}_4 \rightarrow ^3\text{H}_5$	1350
#3	Er:Pr:YSZ	Er: $^4\text{I}_{15/2} \rightarrow ^4\text{I}_{11/2}$	970	Er: $^4\text{I}_{13/2} \rightarrow ^4\text{I}_{15/2}$	1530
		Pr: $^3\text{H}_4 \rightarrow ^1\text{G}_4$	1020	Pr: $^1\text{G}_4 \rightarrow ^3\text{H}_5$	1350

Table 1. Sample reference numbers with their composition, absorption/emission transitions and wavelength.

### 3.2.3. Optical efficiency

Studies of optical efficiency ( $\epsilon$ ) in luminescent samples are of interest for optical applications in order to understand hindering of luminescence by ion-ion interaction and energy transfer. Optical efficiency was calculated by the rate between PL intensity and pumping power of the exciting laser source. In this study, we aimed to compare efficiencies of  $\text{Er}^{3+}$  and  $\text{Pr}^{3+}$  emissions for the three samples excited at their optimal absorption wavelength.

First, we pumped Pr-doped YSZ monolayer and Er-:Pr-doped YSZ superlattice at wavelengths of 1030 and 1020 nm, respectively, to detect light emission at 1350 nm from Pr<sup>3+</sup> ions as a function of the pumping power as schemed in Fig. 9 (a). As observed in measurements in Fig. 9 (b), optical efficiency for Pr:YSZ monolayer ( $\epsilon^{\text{Pr emission}}_{\text{Pr:YSZ}} = 0.53$ ) is slightly higher than for the Er:Pr:doped YSZ superlattice ( $\epsilon^{\text{Pr emission}}_{\text{Er:Pr:YSZ}} = 0.5$ ) at 1350 nm. It can be observed for Er:Pr:YSZ superlattice a saturation of Pr<sup>3+</sup> emission at 1350 nm from pumping power higher than 150 mW, which might suggest an energy transfer between Pr<sup>3+</sup> and Er<sup>3+</sup> ions.



**Figure 9.** (a) Schematics diagram of ground state absorption (GSA) (red) and emission (violet) in the near-IR of Pr<sup>3+</sup> ions energy levels. (b) Optical efficiency for Pr:Er:YSZ (in black) and Pr:YSZ (in violet) and its optical efficiency coefficients.

Secondly, Er:YSZ and Er:Pr:YSZ samples have been pumped at wavelengths of 960 and 970 nm, respectively, to measure Er<sup>3+</sup> emission at 1530 nm (Fig. 10 (a)). Higher efficiency is achieved for Er-doped monolayer ( $\epsilon^{\text{Er emission}}_{\text{Er:YSZ}} = 0.9$ ) in comparison with Er<sup>3+</sup> emission from the Er:Pr:YSZ sample ( $\epsilon^{\text{Er emission}}_{\text{Er:Pr:YSZ}} = 0.84$ ) despite energy transfer from Pr<sup>3+</sup>(<sup>3</sup>P<sub>0</sub>) to Er<sup>3+</sup>(<sup>4</sup>F<sub>7/2</sub>). Decrease in Er<sup>3+</sup> emission efficiency in Er:Pr:YSZ superlattices have origin in ion-ion interaction between Pr<sup>3+</sup> and Er<sup>3+</sup> ions, as result, Er<sup>3+</sup> emission is quenched. Despite quenching effects observed for Er<sup>3+</sup> emission in the superlattice sample, optical efficiency for Er<sup>3+</sup> is higher than efficiency measured for Pr<sup>3+</sup> emission.

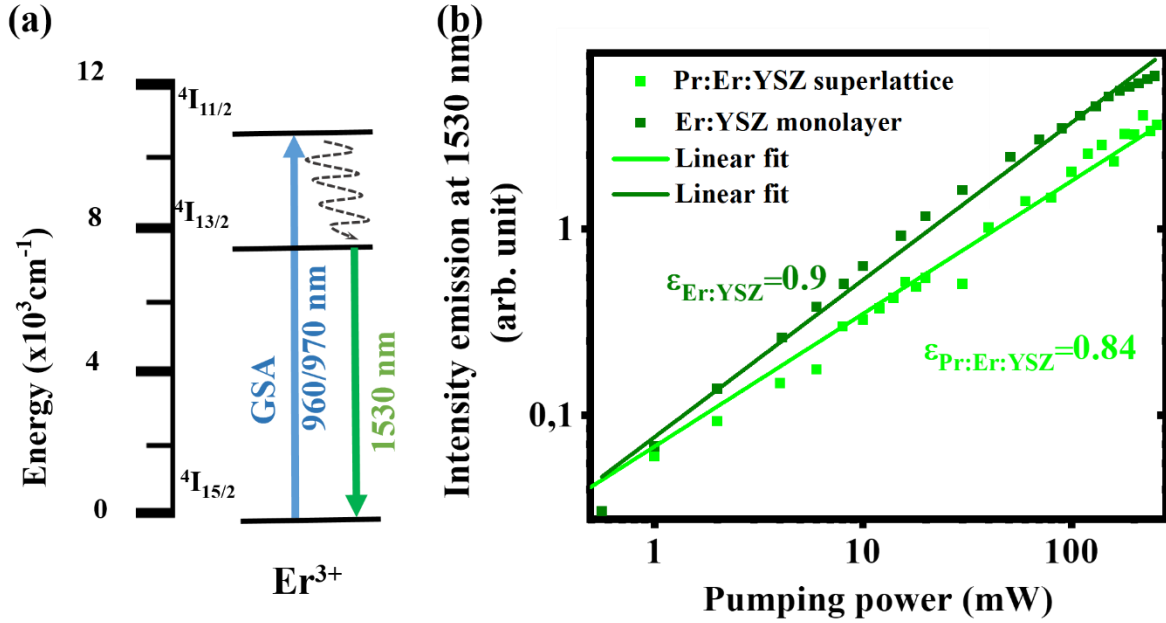


**Figure 10.** (a) Schematics diagram of ground state absorption (GSA) (blue arrow) and emission (green arrow) in the near-IR of  $\text{Er}^{3+}$  ions energy levels. (b) Optical efficiency for Pr:Er:YSZ (light green) and Er:YSZ (dark green) and its optical efficiency coefficients.

As conclusion, it has been noticed lower optical efficiencies for both  $\text{Er}^{3+}$  and  $\text{Pr}^{3+}$  ion emissions in the YSZ superlattice structure in comparison with efficiencies obtained in Er:YSZ and Pr:YSZ monolayers. However,  $\text{Pr}^{3+}$  optical efficiency for both samples containing  $\text{Pr}^{3+}$  ions is very similar:  $\epsilon_{\text{Pr:YSZ}}^{\text{Pr emission}} = 0.53$  for Pr:YSZ and  $\epsilon_{\text{Er:Pr:YSZ}}^{\text{Pr emission}} = 0.5$  for Er:Pr:YSZ superlattice.

In one hand, Er:Pr:YSZ superlattice allows simultaneous emission of both REs at 1530 and 1350 nm by pumping the sample at one wavelength between 970 and 1020 nm. In the other hand the superlattice structure, despite giving a higher control of the interlayer distance and distribution between ions than in other co-doping configurations, is not exempt of quenching effects due to ion-ion interaction. Thus, lower optical efficiency at 1530 and 1350 nm emission wavelengths for Pr:Er-doped superlattice can be explained by means of energy transfer and non-radiative decay between  $\text{Pr}^{3+}$  and  $\text{Er}^{3+}$  ions.

Energy transfer (ET) studies between  $\text{Er}^{3+}$  and  $\text{Pr}^{3+}$  ions in the superlattice sample, we carried out by luminescence lifetime and PL experiments. Lifetime ( $\tau$ ) was measured under  $\text{Pr}^{3+}$  and  $\text{Er}^{3+}$  emission wavelengths of 1350 and 1530 nm, respectively. Reduced luminescence lifetime in Er-Pr-codoped hosts has been observed when adding a second RE dopant to the sample as result of ion-ion interaction [32].

In our experiment, we measured lifetime of  $\text{Pr}^{3+}$  emission transition  $^1\text{G}_4 \rightarrow ^3\text{H}_5$  for Er:YSZ and Er:Pr:YSZ samples (Fig. 11 (a)). While for Pr:YSZ samples, lifetime interaction is restricted to  $\text{Pr}^{3+}$ - $\text{Pr}^{3+}$  ions, for Er:Pr-doped superlattice, lifetime is additionally determined by  $\text{Er}^{3+}$ - $\text{Pr}^{3+}$  ion

interaction. As expected, it has been calculated 0.9 ms lifetime for Pr:YSZ sample excited at 1020 nm. Accordingly, reduced lifetime of 0.6 ms was observed for Er:Pr:YSZ superlattice in which population of the  $^3P_0$  ( $Pr^{3+}$ ) energy level occurs by two-photon absorption by pumping the superlattice sample at 1030 nm [35]. Thus, energy transfer (ET) from ( $Pr^{3+}$ )  $^3P_0$  energy level to lower-lying ( $Er^{3+}$ )  $^4F_{7/2}$  energy level. Depopulation of from  $Er^{3+}$   $^4F_{7/2} \rightarrow ^4I_{15/2}$  energy level involve radiative and nonradiative paths as widely reported in the literature [36, 37]. In this study we had focused in the radiative de-excitation  $^4I_{13/2} \rightarrow ^4I_{15/2}$  of  $Er^{3+}$  corresponding to the emission in the C-band of wavelengths.

Similarly, in Fig. 11 (b) we observe lifetime reduction from 1.9 to 1.5 ms for  $Er^{3+}$  transition emission  $^4I_{13/2} \rightarrow ^4I_{15/2}$  when exciting Er:YSZ and Er:Pr:YSZ samples at 960 and 970 nm, respectively. As observed in  $Pr^{3+}$  decay curves, Er:YSZ thin films measured longer lifetime than Pr:Er:YSZ as result of  $Pr^{3+}$ - $Er^{3+}$  interaction. In this case, for Er:Pr:YSZ superlattice ground state absorption (GSA) transition at 970 nm ( $^4I_{15/2} \rightarrow ^4I_{13/2}$ ) populates the  $^4I_{13/2}$  level, and energy transfer (ET) would be carried out from ( $Er^{3+}$ ):  $^4I_{11/2}$  to the ( $Pr^{3+}$ ):  $^1G_4$  energy levels, lifetime decrease. De-excitations of  $Pr^{3+}$   $^1G_4 \rightarrow ^3H_4$  follow diverse channels of relaxation discussed in different studies [38], although  $Pr^{3+}$  transition  $^1G_4 \rightarrow ^3H_5$  of interest in this work corresponds to the O-band wavelengths.

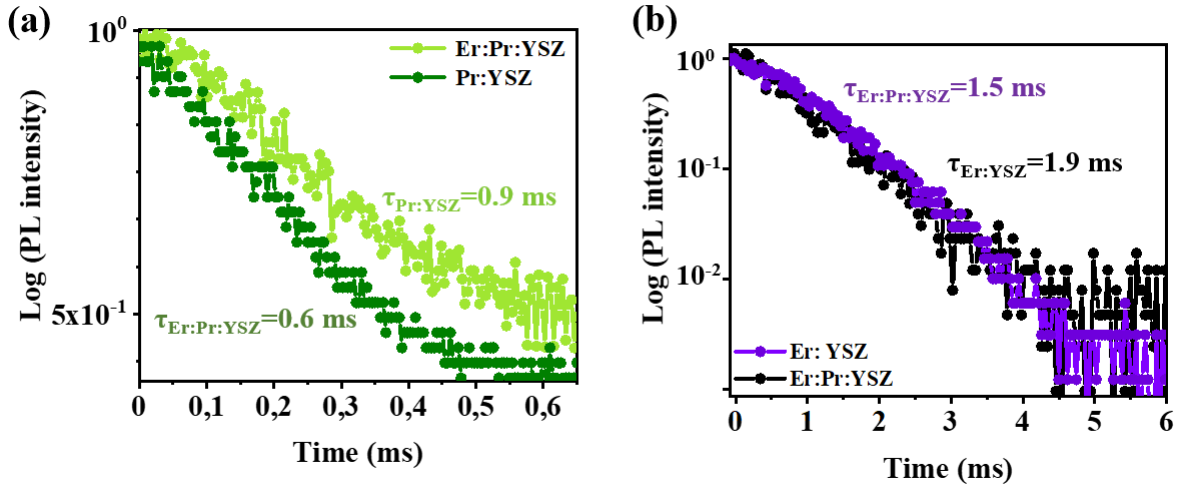


**Figure 11.** Lifetime of (a)  $Pr^{3+}:^1G_4$  transition measured in Pr:YSZ monolayer and Er:Pr:YSZ superlattice and (b)  $Er^{3+}:^4I_{13/2}$  transition measured in Er:YSZ monolayer and Er:Pr:YSZ superlattice.

Complementary, we excited the superlattice sample by PL at the optimal absorption wavelength of RE ion A and measured the emission at the wavelength of RE ion B. In this experiment, we pumped at wavelength of 970 nm characteristic of  $Er^{3+}$  ions absorption, we were not able to detect significant emission of  $Pr^{3+}$  ions at 1350 nm due to signal-to-noise ratio. Meanwhile, at an absorption of  $Pr^{3+}$  ions at 1020 nm wavelength, emission at 1530 nm from  $Er^{3+}$  ions is observed. In Fig. 12 (a) we noticed a mild increase of  $Er^{3+}$  emission when exciting  $Pr^{3+}$  at 1020 nm with increasing power. Expectedly, when exciting Er:YSZ monolayer sample at 1020 nm,  $Er^{3+}$  emission

at 1530 nm has not been detected. Following  $\text{Er}^{3+}$  radiative and non-radiative transitions [39], radiative de-excitation lifetime from  $^4\text{I}_{13/2} \rightarrow ^4\text{I}_{15/2}$  at 1530 nm was measured. Consequently, this results will confirm ET between  $\text{Pr}^{3+}$  and  $\text{Er}^{3+}$  from the ( $\text{Pr}^{3+}$ ):  $^3\text{P}_0$  to the ( $\text{Er}^{3+}$ ):  $^4\text{F}_{7/2}$  energy level as observed in similar studies [40] and as summarized in Fig. 12 (b).

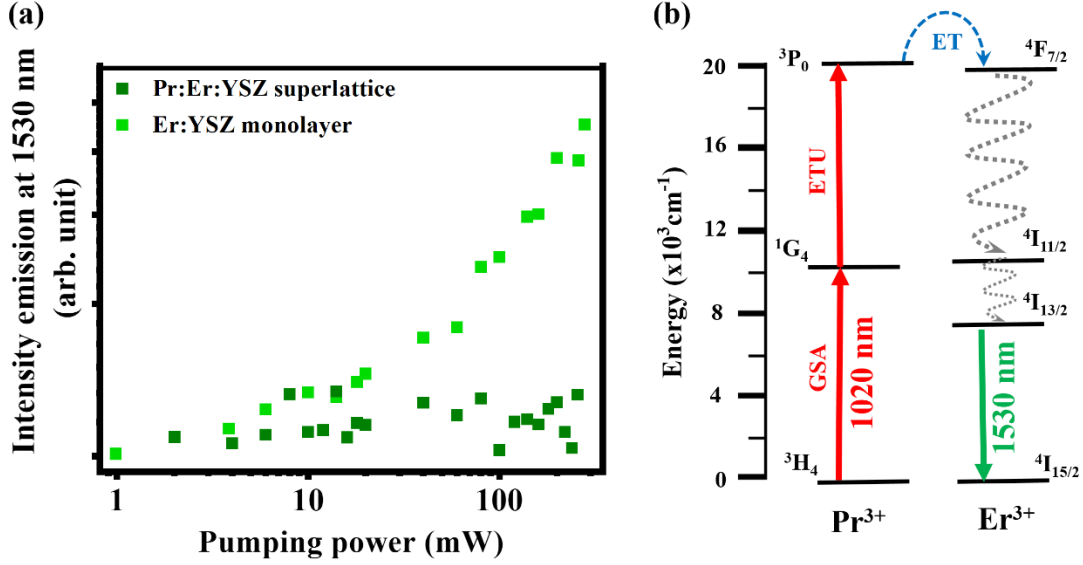


**Figure 12.** (a) Optical efficiency study for  $\text{Er}^{3+}$  emission at 1530 nm from Pr:Er:YSZ (in dark green) and Er:YSZ (light green). (b) Schematic band diagram for  $\text{Pr}^{3+}$  absorption dynamics of energy levels: ground state absorption (GSA) (red) and energy transfer upconversion (ETU), energy transfer (ET) to  $\text{Er}^{3+}$  ions and  $\text{Er}^{3+}$  radiative decay (green).

#### 4. Conclusions

In this work we have grown 150 nm-thick Er:YSZ monolayer, Pr:YSZ monolayer and 300 nm-thick Er:Pr:YSZ superlattice thin films by PLD. We structurally characterized the samples by XRD obtaining two different crystalline orientations (111) and (001) of YSZ cubic phase.

Optical characterization by means of PL proved shifted absorption wavelengths for same  $\text{Er}^{3+}$ :  $^4\text{I}_{15/2} \rightarrow ^4\text{I}_{11/2}$  and  $\text{Pr}^{3+}$ :  $^3\text{H}_4 \rightarrow ^1\text{G}_4$  transitions in Er:YSZ, Pr:YSZ and Er:Pr:YSZ superlattices samples. Indeed, for  $\text{Er}^{3+}$ :  $^4\text{I}_{15/2} \rightarrow ^4\text{I}_{11/2}$  transition, optimal absorption wavelength for Er:YSZ monolayer was found at 960 nm, while for Er:Pr:YSZ superlattice layer at 970 nm. For  $\text{Pr}^{3+}$  transitions  $^3\text{H}_4 \rightarrow ^1\text{G}_4$ , Pr:YSZ and Er:Pr:YSZ optimal absorption wavelengths are obtained at 1030 and 1020 nm, respectively.

In the Er:Pr:YSZ superlattice sample, two transitions  $\text{Pr}^{3+}$ :  $^1\text{G}_4 \rightarrow ^3\text{H}_5$  and  $\text{Er}^{3+}$ :  $^4\text{I}_{13/2} \rightarrow ^4\text{I}_{15/2}$  were measured and analyzed under excitation wavelengths between 970 and 1020 nm. While Er:Pr:YSZ

sample only presents one emission signal under pump wavelength of 970 and 1020 nm for Er<sup>3+</sup> and Pr<sup>3+</sup> emission, respectively, simultaneously light emission at 1530 and 1350 nm is achieved from both Er<sup>3+</sup> and Pr<sup>3+</sup> ions, by exciting the Er:Pr:YSZ superlattice sample at a single wavelength (980 or 1000 nm). Optical studies demonstrated higher Er<sup>3+</sup> and Pr<sup>3+</sup> PL efficiency ( $\epsilon_{\text{Er:YSZ}} = 0.9$  and  $\epsilon_{\text{Pr:YSZ}} = 0.53$ ) in monolayer samples (Er:YSZ and Pr:YSZ) in comparison with same ion emission in Er:Pr:YSZ superlattice ( $\epsilon^{\text{Er emission}}_{\text{Er:Pr:YSZ}} = 0.84$  and  $\epsilon^{\text{Pr emission}}_{\text{Er:Pr:YSZ}} = 0.5$ ). Finally, two energy transfers from Pr<sup>3+</sup> /Er<sup>3+</sup> ions were revealed by measuring decreasing lifetimes for Pr<sup>3+</sup> and Er<sup>3+</sup> emissions in Er:Pr:YSZ sample in comparison with Er:YSZ and Pr:YSZ emissions. Reduction in lifetimes calculations suggests energy transfer in superlattice sample from (Pr<sup>3+</sup>:) <sup>3</sup>P<sub>0</sub> to (Er<sup>3+</sup>:) <sup>4</sup>F<sub>7/2</sub> and from (Er<sup>3+</sup>:) <sup>4</sup>I<sub>13/2</sub> to (Pr<sup>3+</sup>:) <sup>1</sup>G<sub>4</sub> energy levels.

This study demonstrates the capability of crystalline oxides to be doped with RE in compact superlattice structures in which quenching effects could be controlled by ion-ion interdistances. Moreover, dual wavelength emission of two different telecommunication bands offers new perspectives and versatility by increasing the operating wavelength in hybrid integrated devices such as sensors optical amplifiers in silicon platforms.

## Acknowledgements

This work has received the funding from the European Research Council (ERC) under the European Union's Horizon 2020 Research and Innovation Program (ERC POPSTAR – grant agreement No 647342) and ANR FOIST project. The authors thank the French RENATECH network for its support in cleanroom activities.

## References

- [1] F. Testa, A. Bianchi, S. Stracca, R. Sabella, Silicon Photonics for Telecom and Datacom Applications. Silicon Photonics III (2016) 421-446.
- [2] S. Pitris, M. Moralis-Pegios, T. Alexoudi, Y. Ban, P. De Heyn, J. Van Campenhout, J., Lambrecht, H. Ramon, X. Yin, J. Bauwelinck, N. Pleros, N., O-band silicon photonic transmitters for datacom and computercom interconnects, J. Light. Technol. 37(19) (2019) 5140-5148.
- [3] B.R. Koch, E.J. Norberg, J.E. Roth, B. Kim, A. Ramaswamy, R.S. Guzzon, J. Hutchinson, J.H. Shin, J. Imamura, B. Gomez, G. Fish, Heterogeneously integrated lasers on silicon. In Novel In-Plane Semiconductor Lasers XIII (9002, 90020U). International Society for Optics and Photonics (2014).
- [4] D.J. Lockwood, L. Pavesi, Silicon Fundamentals for Photonics Applications. In: Silicon Photonics. Topics in Applied Physics, 94. (2004) Springer, Berlin, Heidelberg.
- [5] N. Daldosso, L. Pavesi, L., Nanosilicon photonics. Laser Photonics Rev., 3(6) (2009) 508-534.
- [6] A.J. Kenyon, Recent developments in rare-earth doped materials for optoelectronics. Prog. Quantum Electron. , 26(4-5) (2002) 225-284.,

- [7] L.H. Slooff, A. Van Blaaderen, A. Polman, G.A. Hebbink, S.I. Klink, F.C.J.M Van Veggel, D.N. Reinhoudt, J.W. Hofstraat, Rare-earth doped polymers for planar optical amplifiers. *J. Appl. Phys.*, 91(7) (2002) 3955-3980.
- [8] M.K. Hossain, M.H. Ahmed, M.I. Khan, M.S. Miah, S. Hossain, *ACS Appl. Electron. Mater.*, 3(10) (2021) 4255–4283.
- [9] W.F. Meggers, Emission Spectra of the Rare Earth Elements, *J. Opt. Soc. Am.* 31 (1941) 157-159
- [10] Y. Durteste, M. Monerie, J.Y. Allain, H. Poignant, Amplification and lasing at 1.3  $\mu\text{m}$  in praseodymium-doped fluorozirconate fibres. *Electron. Lett.* 27(8) (1991) 626-628.
- [11] T.J. Whitley, A review of recent system demonstrations incorporating 1.3- $\mu\text{m}$  praseodymium-doped fluoride fiber amplifiers. *J. Light. Technol.*, 13(5) (1995)744-760.
- [12] Q. Sheng, X. Wang, D. Chen, Near-infrared emission from Pr-doped borophosphate glass for broadband telecommunication. *J. Lumin.*, 135 (2013)38-41.
- [13] C. Khurmi, S. Thoday, T.M. Monro, G. Chen, D.G. Lancaster, Visible laser emission from a praseodymium-doped fluorozirconate guided-wave chip. *Opt. Lett.*, 42(17) (2017) 3339-3342.
- [14] J. D. B. Bradley, M. Pollnau, Erbium-doped integrated waveguide amplifiers and lasers. *Laser Photonics Rev.*, 5(3) (2010) 368–403.
- [15] J. Mu, M. Dijkstra, J. Korterik, H. Offerhaus, S.M. García-Blanco, "High-gain waveguide amplifiers in  $\text{Si}_3\text{N}_4$  technology via double-layer monolithic integration," *Photon. Res.* 8 (2020)1634-1641
- [16] J. Rönn, W. Zhang, A. Autere, X. Leroux, L. Pakarinen, C. Alonso-Ramos, A. Säynätjoki, H. Lipsanen, L. Vivien, E. Cassan, Z. Sun, Ultra-high on-chip optical gain in erbium-based hybrid slot waveguides. *Nat. Commun.*, 10(1) (2019).
- [17] G.S. Li, C.M. Zhang, P.F. Zhu, C. Jiang, P. Song, K. Zhu, Broadband near-infrared emission in  $\text{Pr}^{3+}$ - $\text{Er}^{3+}$  codoped phosphate glasses for optical amplifiers. *Ceram. Int.*, 42(4) (2016) 5558-5561.
- [18] X. Shen, Y. Zhang, L. Xia, J. Li, G. Yang, Y. Zhou, Dual super-broadband NIR emissions in  $\text{Pr}^{3+}$ - $\text{Er}^{3+}$ - $\text{Nd}^{3+}$  tri-doped tellurite glass. *Ceram. Int.*, 46(9) (2020)14284-14286
- [19] G. Lakshminarayana, I.V. Kityk, M.A Mahdi, K.J Plucinski, Er/Pr-codoped borotellurite glasses as efficient laser operated nonlinear optical materials. *Mater. Lett.*, 214 (2018)23-25.
- [20] Q. Xu, Y. Wang, F. Chen, W. Wong, Z. Zhang, D. Zhang,  $\text{Er}^{3+}$  cross-section spectra of  $\text{Er}^{3+}/\text{Pr}^{3+}:\text{Gd}_3\text{Ga}_5\text{O}_{12}$  single-crystal:  $\text{Pr}^{3+}$ -codoping effect. *J. Am. Ceram. Soc.*, 102(11), (2019) 6407–6413.
- [21] D. J. Coleman, P. Golding, T. King, S. D. Jackson, Spectroscopic and energy-transfer parameters for  $\text{Er}^{3+}$ -doped and  $\text{Er}^{3+}$ ,  $\text{Pr}^{3+}$ -codoped GeGaS glasses. *J. Opt. Soc. Am. B*, 19(9) (2002) 1982.
- [22] D.W. Bruce, D. O'Hare, R.I. Walton, eds., 2011. *Functional oxides* (Vol. 12). John Wiley & Sons.
- [23] F. Ockenfuß, W. Baudenbacher, K. Prusseit-Elffroth, P. Hirata, H. Berberich, Kinder, Preparation and growth of YSZ buffer layers and  $\text{YBa}_2\text{Cu}_3\text{O}_7$ -films on silicon (100). *Physica C Supercond.*, 180(1-4) (1991) 30-33.
- [24] Z. Xiao, S. Yu, Y. Li, S. Ruan, L.B. Kong, Q. Huang, Z. Huang, K. Zhou, H. Su, Z. Yao, W. Que, Y. Liu, T. Zhang, J. Wang, P. Liu, D. Shen, M. Allix, J. Zhang, D. Tang, Materials development and potential applications of transparent ceramics: A review, *Mater. Sci. Eng. R Rep.*, 139 (2020) 100518, ISSN 0927-796X.

- [25] N. Nicoloso, A. Löbert, B. Leibold, Optical absorption studies of tetragonal and cubic thin-film yttria-stabilized zirconia, *Sens. Actuators B Chem.*, 8(3) (1992) 253-256, ISSN 0925-4005
- [26] G. Marcaud, S. Matzen, C. Alonso-Ramos, X. Le Roux, M. Berciano, T. Maroutian, G. Agnus, P. Aubert, L. Largeau, V. Pillard, S. Serna, D. Benedikovic, C. Pendenque, E. Cassan, D. Marris-Morini, P. Lecoeur, L. Vivien, High-quality crystalline yttria-stabilized-zirconia thin layer for photonic applications. *Phys. Rev. Mater.*, 2(3) (2018) 035202.
- [27] A. Ruiz-Caridad, G. Marcaud, E. Duran-Valdeiglesias, J.M. Ramirez, J. Zhang, C. Alonso-Ramos, X. LeRoux, L. Largeau, S. Serna, N. Dubreuil, S. Matzen, T. Maroutian, P. Lecoeur, D. Marris-Morini, E. Cassan, L. Vivien. Heterogeneous Integration of Doped Crystalline Zirconium Oxide for Photonic Applications, in *IEEE Journal of Selected Topics in Quantum Electronics*, 28, (3) (2022) 1-13.
- [28] H.G. Scott, Phase relationships in the zirconia-yttria system. *J. Mater. Sci.*, 10(9) (1975) 1527-1535.
- [29] H. Hidalgo, E. Reguzina, E. Millon, A. L. Thomann, J. Mathias, C. Boulmer-Leborgne, T. Sauvage, P. Brault, Yttria-stabilized zirconia thin films deposited by pulsed-laser deposition and magnetron sputtering. *Surf. Coat. Technol.*, 205(19) (2011) 4495-4499.
- [30] B. Savoini, J.E. Muñoz-Santiuste, R. González, G.K. Cruz, C. Bonardi, R.A. Carvalho, Upconversion luminescence of Er<sup>3+</sup>-doped YSZ single crystals. *J. Alloys Compd*, 323 (2001) 748-752.
- [31] B. Zhou, L. Tao, Y. H. Tsang, W. Jin, E. Y. Pun, Superbroadband near-IR photoluminescence from Pr<sup>3+</sup>-doped fluorotellurite glasses, *Opt. Express*, 20 (2012) 3803-3813.
- [32] W. A. Pisarski, J. Pisarska, M. Kuwit, M. Kochanowicz, J. Zmojda, P. Miluski, A. Baranowska, J. Dorosz M. Lesniak, D. Dorosz, Fluoroindate glasses co-doped with Pr/Er for near-infrared luminescence applications. *Sci. Rep.*, (2020), 10:21105.
- [33] C. A. Morrison, Host dependence of the rare-earth ion energy separation 4f N–4f N–1 nl, *J. Chem. Phys.*, 72 (1980) 1001-1002.
- [34] A.A. Bagatur'yants, I.M. Iskandarova, A.A. Knizhnik, V.S. Mironov, B.V. Potapkin, A.M. Srivastava, T.J. Sommerer, Energy level structure of 4 f 5 d states and the Stokes shift in LaPO<sub>4</sub>:Pr<sup>3+</sup>: A theoretical study. *Phys. Rev. B Condens. Matter*, 78(16) (2008) 165125.
- [35] G.A. Kumar, E. De la Rosa, H. Desirena, Radiative and non-radiative spectroscopic properties of Er<sup>3+</sup> ion in tellurite glass. *Opt. commun.* 260(2) (2006) 601-606.
- [36] A., Polman, Erbium as a probe of everything?. *Phys. B: Condens. Matter*, 300(1-4) 2001. 78-90.
- [37] R. Piramidowicz, R. Mahiou, P. Boutinaud, M. Malinowski. Upconversion excitations in Pr<sup>3+</sup>-doped BaY<sub>2</sub>F<sub>8</sub> crystal. *Appl. Phys. B* 104 (2011) 873–881.
- [38] B. Savoini, J.M. Santiuste, R. and Gonzalez, Optical characterization of Pr<sup>3+</sup>-doped yttria-stabilized zirconia single crystals. *Phys. Rev. B*, 56(10) (1997) 5856.
- [39] E. Greenberg, G. Katz, R. Reisfeld, N. Spector, R.C. Marshall, B. Bendow, R.N. Brown, Radiative transition probabilities of Er<sup>3+</sup> in yttria stabilized cubic zirconia crystals. *The J. Chem. Phys.*, 77(10) (1982) 4797-4803.
- [40] P. Feng, X. Wang, Y. Zhao, D.C. Fang, X. Yang, Energy transfer between rare earths in layered rare-earth hydroxides, *RSC Adv.*, 2018, 8(7), 3592-3598.